S-wave Velocity Model Estimation using Ambient Seismic Noise at Virgo, Italy

Soumen Koley[*1], *Henk Jan Bulten* [1], *Jo van den Brand* [1], *Maria Bader* [1], *Xander Campman* [2], *Mark Beker* [3]
[1] *National Institute of Subatomic Physics, Amsterdam,* [2] *Shell Global Solutions International B.V. Netherlands,*
[3] *Innoseis B.V. Netherlands*

SUMMARY

In this study, we present an analysis of seismic noise recorded at the Virgo gravitational wave detector in Italy. The study originates from the need to understand the spatio-spectral characteristics of the seismic noise at the Virgo site. Studying the direction of propagation and Rayleigh wave phase velocities of possible noise sources is of utmost importance for accurate computation of Newtonian noise, which appears to be the ultimate low frequency limit for ground based gravitational wave detectors. For this purpose, a seismic array was designed that would ensure correct estimation of phase velocities and propagation direction of ambient seismic noise in the frequency range $0.4-8.0$ Hz. Consequently, a passive seismic survey was carried out using a network of 5 Hz vertical component wireless geophones at the site between 13-28 August 2016. The $0.2-0.7$ Hz frequency band was dominated by the secondary microseismic energy originating from the Mediterranean sea. A strong correlation was observed between the microseismic energy and the significant wave height in the Mediterranean sea during the time. Seismic noise in the frequency band $1.5-4.0$ Hz was dominated by ground motions induced in the subsurface by road bridges and local traffic activities. In the $4-8$ Hz band, noise sources were mostly local and transient. The direction of propagation of the ambient noise was estimated using beamforming. To estimate the phase velocities, both beamforming and extended spectral autocorrelation (ESAC) were used. Using the derived Rayleigh wave phase velocity corresponding to the fundamental mode, an inversion was carried out to estimate a 1-D S-wave velocity model for the region. Subsurface properties obtained from the study can be further used for computing the gravity gradient noise associated with seismic motions in the region.

INTRODUCTION

Gravitational Wave detectors work on the principle of Michelson Interferometer (Saulson, 1994) and are capable of measuring tiny ripples in space-time in the order of 10^{-18} m. The gravitational wave detector at Virgo comprises two 3 km long orthogonal arms with high reflective mirrors at the ends. A beam of light is split and made to travel separately along each arm of the interferometer. After reflection from the end mirrors, they recombine at the beam splitter and an interference pattern is observed. If a gravitational wave passes through the interferometer, it causes changes to the interference pattern. To attain sensitivities to such small strains, it is important to isolate the suspended elements of the system (beam splitter and the end mirrors) from seismic motions. The detector at Virgo makes use of advanced techniques in seismic isolation (Acernese et al., 2010) to overcome these problems. However, the seismic attenuators fail to isolate the system from very low frequency ground motions. In addition, these seismic motions also cause displacement of the subsurface elements, leading to a change in the gravitational force between the suspended elements and the subsurface. Hence, a change in the equilibrium position of the suspended elements. This noise is generally referred to as the gravity gradient noise or the Newtonian noise (Hughes and Thorne, 1998). In the context of these detectors, there are two important implications of ambient seismic noise measurements carried out at Virgo. Firstly, it helps us identify the seismic noise sources at low frequencies, and secondly using these measurements we can obtain a near surface S-wave velocity model in the region, which can be further used for simulations involving Newtonian noise subtraction.

SEISMIC ARRAY DESIGN

Designing seismic arrays for studying the phase velocities and the direction of propagation of ambient noise, pose conflicting restrictions on the selection of intersensor spacing. Larger intersensor separation helps increase the resolution of phase velocity estimates for long period waves, while smaller intersensor distances prevents the high frequency waves from getting spatially aliased. We make use of the concept of Theoretical Array Response introduced by Woods and Lintz (1973) to design a seismic array that works well in the $0.4-8.0$ Hz frequency band. Given a set of M sensors, with location coordinates $[(x_0,y_0),(x_1,y_1),...(x_{m-1},y_{m-1})]^T$, the array response vector or the steering vector $a(f)$ can be expressed as,

$$a(f) = [e^{-j2\pi f\tau_0}, e^{-j2\pi f\tau_1}, ...e^{-j2\pi f\tau_{m-1}}]^T \quad (1)$$

$\tau_m = x_m p\cos\phi + y_m p\sin\phi$ is the time delay for signal to reach the m^{th} sensor from the origin, and p, ϕ are the slowness and the angle of propagation (always measured anti-clockwise from East) respectively. Given there are N_p values of slowness, and N_ϕ values of azimuth, the total number of steering vectors that can be constructed is N_pN_ϕ. Thus, we can define the array response matrix as,

$$A(f) = [a_1(f), a_2(f).....a_{N_pN_\phi}(f)] \quad (2)$$

Where each column of the matrix is constituted of one particular steering vector. For a plane wave impinging the array along an azimuth ϕ_k and propagating with slowness p_k, the theoretical response $AR_k(f)$ of the array at frequency f is then defined as,

$$AR_k(f) = \frac{1}{N_pN_\phi}\, A(f)\, a_k^*(f) \quad (3)$$

$a_k^*(f)$ represents the complex conjugate, and the quantity $1/N_pN_\phi$ normalizes the maximum value of the array response to 1.

From equation 3, it can be concluded that the theoretical array response attains a maximum value close to 1 for the steering vector that most closely resembles the actual propagation direction and slowness. All other combinations of the inner product between the steering vector and columns of the array response matrix contribute to smaller lobes surrounding the main peak in $p-\phi$ domain. An ideal array should be able to suppress such side lobes to reasonably low magnitudes, relative to the peak value. The theoretical array response for several sensor geometries was tested and a geometry with seismic sensors placed along concentric rings was found the most suitable. The geometry is composed of 8 concentric rings (Figure 1) of radii, $6, 12, 24, 48, 96, 192, 768, 1536$ m respectively. The number of sensors from the innermost to the outermost ring varied as, 1(center), $3, 5, 7, 9, 11, 13, 15$. Alternate sensors in the penultimate ring was also shifted by a distance of 100 m, to achieve a better distribution of interstation distances. The designed array is characterized by a maximum aperture of ≈ 3000 m, and hence can sample low frequency events. The smaller intersensor separation in the inner rings prevents the high frequency events from getting spatially aliased. A circular geometry also ensures azimuthal symmetry. Figure 2 shows the theoretical array responses at the lowest and the highest frequency of interest for a plane wave propagating along an azimuth of 135 ^{0}, and velocities of 2000 and 200 m/s respectively. The radial axis in Figure 2 is slowness p in units of s/m and the azimuth ϕ is measured anticlockwise from the x-axis.

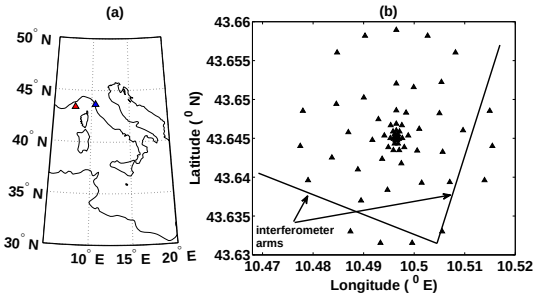

Figure 1: (a) The blue and the red triangle points to the array locations and the Côte d'Azur Buoy respectively. (b) Sensor Layout along with orientation of the interferometer arms

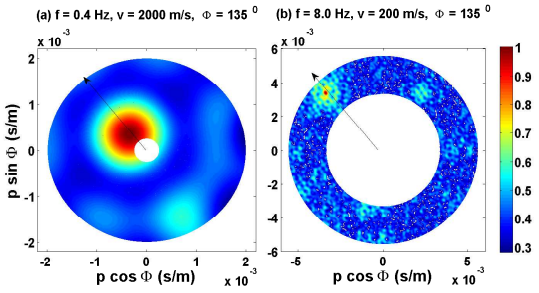

Figure 2: Theoretical Array response at (a) $f = 0.4$ Hz, and (b) $f = 8.0$ Hz

PASSIVE SEISMIC SOURCES

Seismic noise recorded at Virgo can be categorized into three different frequency bands, namely the oceanic microseism ($0.4-0.8$ Hz), road bridge noise ($1.5-4.0$ Hz) and local sources ($4-8$ Hz).

Oceanic Microsiesm

During the 16 days of measurement, we classified the microseismic energy into three types of events, namely A, B and C. Figure 3(a) shows the estimated power spectral density (PSD) for one of the stations. Type A event observed during 13-15 August, is characterized by low microseismic energy and a peak frequency between $0.6-0.8$ Hz. Consequently, the significant wave height in the Mediterranean sea obtained from the Côte d'Azur Buoy (43.38 ^0N, 7.83 ^0E, depth of anchoring 2300 m) was observed to be < 0.5 m as shown in Figure 3(b). The peak frequency of the microseism shifts to frequencies between $0.3-0.4$ Hz for event B recorded during 16-19 August. This shift in frequency can be attributed to a higher wave height of ≈ 1.0 m recorded during the same period. Event C observed between 21-22 August sees a moderate storm pass through the Mediterranean and significant wave height of ≈ 1.5 m. The peak frequency as a result shifts between $0.3-0.4$ Hz along with a minor peak in the frequency range $0.2-0.3$ Hz. Overall a good correlation between the swell in the Mediterranean and the microseismic energy was observed. However, since the location of the buoy and the sensors was ≈ 200 km apart, a slight delay between the changes in the wave height and changes in the microseismic energy was noted.

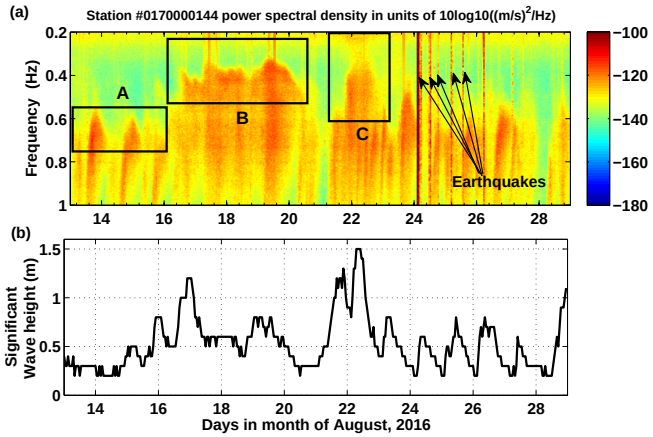

Figure 3: (a) Estimated Power Spectral Density in the frequency range $0.2-1.0$ Hz between 13-28 August 2016. (b) Significant wave height (m) during the same period recorded at Côte d'Azur buoy.

Road Bridge Noise

Five road bridges located within distances of 4 km from the interferometer arms were identified to be possible sources of noise in the frequency range $1.5-4.0$ Hz. Figure 4 (a) shows

the locations of the bridges on a map, along with the interferometer arms. Bridges A1, A2, B and D which are located about 1.5 km away from the interferometer ends, had the maximum contribution to the noise observed at the site. The bridges induce oscillations in the ground in the frequency range $1.5-4.0$ Hz and $5.5-8.0$ Hz. However, only the low frequency component of the noise propagates to Virgo, while the high frequency is attenuated much earlier (Acernese et al., 2004). Figure 5 shows the PSD of the recorded signal beneath bridge A1 and that recorded at the central building. A strong correlation was observed in the low frequency region.

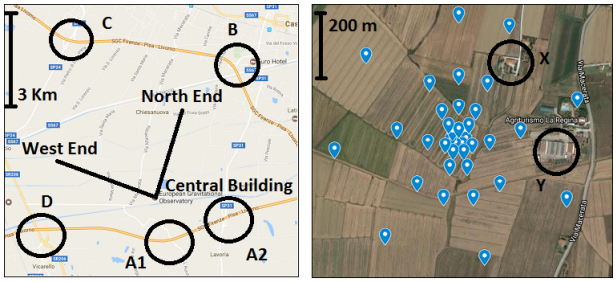

Figure 4: (a) Location of the road bridges near the Virgo site. (b) Blue balloons show the sensor distribution in the center of the array along with the local noise sources ($4-8$ Hz) marked as X and Y

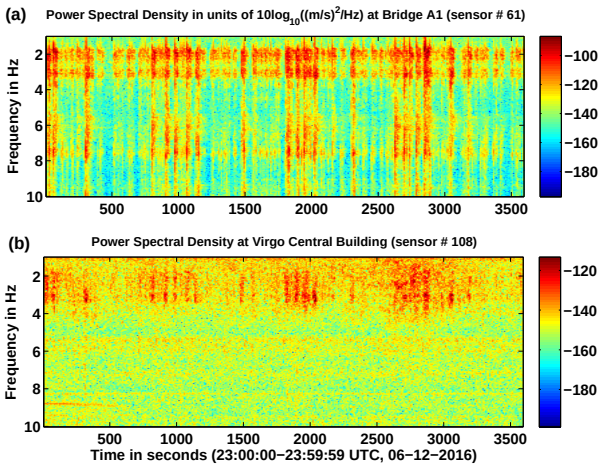

Figure 5: (a) Estimated PSD beneath bridge A1, and (b) at the Virgo Central building

Local Noise Sources

In the high frequency band $4-8$ Hz, noise sources are mostly local and transient, and attenuate over small propagation distances. Hence, a dense network of 25 sensors in the center of the array (Figure 4 (b)) are used for phase velocity estimation. For example Figure 6 shows a noise gather recorded by the sensors in the center of the array that was used in the analysis. Other miscellaneous noise sources in this frequency range include ground motion induced by shaking of local structures during periods of high wind speed.

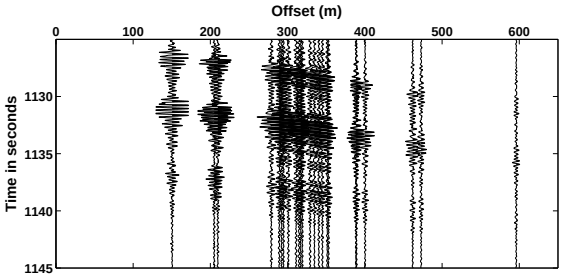

Figure 6: A noise gather from a source originating in the central part of the array in the range $4-8$ Hz

PHASE VELOCITY AND PROPAGATION DIRECTION

A frequency domain beamforming method is implemented to estimate the phase velocities and directions of propagation. Conventional beamforming methods based on Lacoss et al. (1969) makes use of the data covariance matrix to obtain the power associated with a steering vector. In time domain it can be interpreted as a simple method of delay and sum. The power of the stacked signal essentially gives us information about the correctness of the delay applied and is often referred to as the beampower. The Beampower ($BP(f)$) corresponding to a steering vector $a_k(f)$ is computed as,

$$BP(f) = a_k^*(f) R_{xx}(f) a_k(f) \tag{4}$$

Where, $R_{xx} = X(f)X^*(f)$ is the frequency domain data covariance matrix. The oceanic microseism is analyzed in one-hour records and then stacked over a day of measurement. Figure 7 shows the beamforming output for August 18, 2016. Phase velocities range from $2-0.7$ km/s in the $0.4-1.0$ Hz band. The propagation azimuth is $\approx 180^0$ (measured anticlockwise from the east) and can be attributed to the waves in the Mediterranean sea hitting the coast of Pisa.

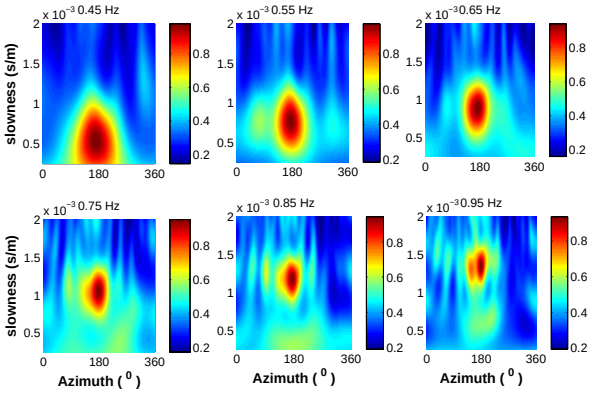

Figure 7: Beamforming output showing normalized beampower as a function of slowness and azimuth for August 18, 2016 at frequencies between $0.45-0.95$ Hz

Beamforming was also performed on the data in the range $1.5-4.0$ Hz, to validate the direction of propagation of the road bridge noise. Unlike the oceanic microseism, smaller

segments of data (300 s) were processed at a time and then stacked over every hour. Figure 8 shows the beamforming output for an hour of data in the frequency band $1.5-4.0$ Hz. The noise source during the time was due to bridge B and hence a propagation azimuth of $\approx 50^0$ is observed. Similar analysis is performed for the frequency range $4.0-8.0$ Hz. Due to the localized nature of the high frequency noise sources only the 25 sensors in the center of the array are used for phase velocity estimation. Figure 9 shows the Rayleigh wave phase velocity dispersion curve estimated for the entire frequency band of $0.4-8.0$ Hz.

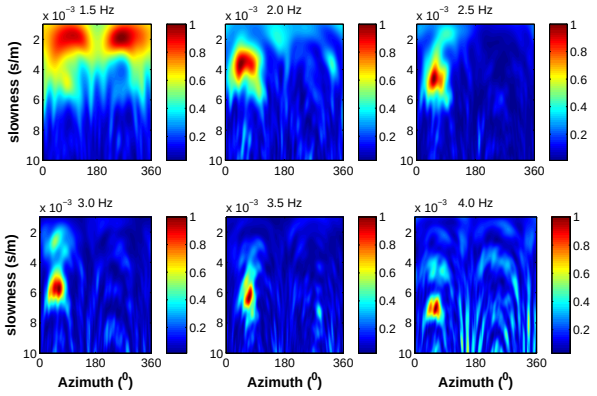

Figure 8: Beamforming output showing normalized beampower as a function of slowness and azimuth for August 13, 2016, 04:00:00-04:59:59 UTC at frequencies between $1.5-4.0$ Hz

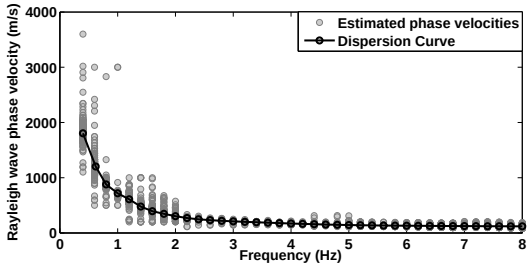

Figure 9: Rayleigh wave phase velocity dispersion curve

DISPERSION CURVE INVERSION

The Rayleigh wave phase velocity curve is inverted to obtain a 1-D S-wave velocity model of the region. The inversion is carried out using the method proposed in Wathelet et al. (2004). The forward problem of computing the theoretical dispersion curve is accomplished using the Thomson-Haskell propagator matrix method (Haskell, 1953). The inversion scheme is an implementation of the neighborhood algorithm pertaining to a multidimensional parameter space (Sambridge, 1999). In the context of Rayleigh wave phase velocity inversion, the parameters are the P-wave, S-wave velocities, density and thickness of each layer in the model. Generally, such inverse problems are not sensitive enough for reliable estimation of the P-wave velocities and the density. Hence, we fix the values of density for each layer based on a priori information. Subsurface geology at Virgo, is well studied through boreholes and gravimetric measurements (Stefanelli et al., 2008) to a depth of 70 m. The upper 70 m of subsurface was formed mainly due to glacial activity and eustatic changes during Pleistocene period and comprise four distinct layers, namely shallow mud and clay (1.5 gm/cc), sands (1.7 gm/cc), gravel (2.1 gm/cc), and organic clay (1.6 gm/cc). MASW studies have also been carried out in the region previously, near the central building, the north end and the west end of the interferometer. Based on these studies, the inversion is carried out assuming a 9 layer velocity model. Figures 10(a) and (b) shows the velocity models explored and the corresponding dispersion curves with misfit values shown in the colorbar. Figure 10(c) shows a comparison of the V_s model obtained from this study with the estimated velocity models from previous MASW measurements.

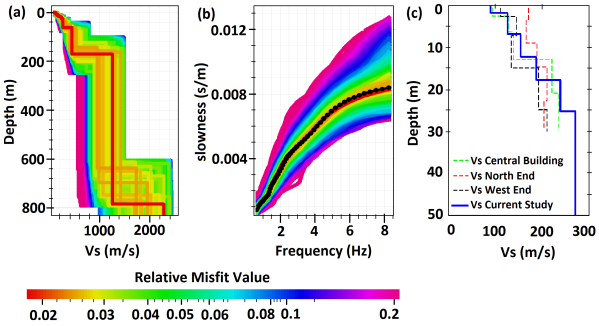

Figure 10: (a) S-wave velocity models explored for a 9 layer model, with red line showing the best model having minimum misfit (b) Theoretical dispersion curves corresponding to all explored models in (a) and the observed dispersion curve (black) (c) V_s model from this study and previous MASW measurements for top 50 m

CONCLUSION

In this paper, we demonstrated the use of surface wave methods for understanding the direction of propagation and phase velocities of the ambient seismic noise sources in the $0.4-8.0$ Hz frequency band. Apart from the oceanic microseismic energy, important noise sources like that of the road bridges were identified, and subsequently used for phase velocity computation. The use of wireless seismic sensors significantly contributed to the design of an optimal array that was able to sample the seismic noise over a broad frequency range. The inverted S-wave velocity model gives us information up to a depth 800 m, which matches well with the presence of a carbonate bedrock at that depth. The top 50 m of the derived S-wave model was also in good agreement with previous MASW measurements at Virgo.

EDITED REFERENCES

Note: This reference list is a copyedited version of the reference list submitted by the author. Reference lists for the 2017 SEG Technical Program Expanded Abstracts have been copyedited so that references provided with the online metadata for each paper will achieve a high degree of linking to cited sources that appear on the Web.

REFERENCES

Acernese, F., P. Amico, N. Arnaud, D. Babusci, R. Barill´e, F. Barone, L. Barsotti, M. Barsuglia, F. Beauville, M. Bizouard, et al.,2004, Properties of seismic noise at the virgo site: Classical and Quantum Gravity, **21**, S433, http://dx.doi.org/10.1088/0264-9381/21/5/008.

Acernese, F., F. Antonucci, S. Aoudia, K. Arun, P. Astone, G. Ballardin, F. Barone, M. Barsuglia, T. S. Bauer, M. Beker, et al.,2010, Measurements of superattenuator seismic isolation by virgo interferometer: Astroparticle Physics, **33**, 182–189, http://dx.doi.org/10.1016/j.astropartphys.2010.01.006.

Haskell, N. A., 1953, The dispersion of surface waves on multilayered media: Bulletin of the seismological Society of America, **43**, 17–34.

Hughes, S. A., and K. S. Thorne, 1998, Seismic gravity-gradient noise in interferometric gravitational-wave detectors: Physical Review D, 58, 122002, http://dx.doi.org/10.1103/PhysRevD.58.122002.

Lacoss, R. T., E. J. Kelly, and M. N. Toksöz, 1969, Estimation of seismic noise structure using arrays: Geophysics, **34**, 21–38, http://dx.doi.org/10.1190/1.1439995.

Sambridge, M., 1999, Geophysical inversion with a neighbourhood algorithm II. appraising the ensemble: Geophysical Journal International, **138**, 727–746, http://dx.doi.org/10.1046/j.1365-246x.1999.00900.x.

Saulson, P. R., 1994, Fundamentals of interferometric gravitaional wave detectors: World Scientific.

Stefanelli, P., C. Carmisciano, F. Caratori Tontini, L. Cocchi, N. Beverini, F. Fidecaro, and D. Embriaco, 2008, Microgravity vertical gradient measurement in the site of virgo interferometric antenna (pisa plain, italy): Annals of Geophysics.

Wathelet, M., D. Jongmans, and M. Ohrnberger, 2004, Surface-wave inversion using a direct search algorithm and its application to ambient vibration measurements: Near surface geophysics, **2**, 211–221, http://dx.doi.org/10.3997/1873-0604.2004018.

Woods, J. W., and P. R. Lintz, 1973, Plane waves at small arrays: Geophysics, **38**, 1023–1041, http://dx.doi.org/10.1190/1.1440393.